Intercalation processes and diffusion paths of lithium ions in spinel-type structured $Li_{1+x}Ti_2O_4$: Density functional theory study

M. Anicete-Santos,[1,2] L. Gracia,[1] A. Beltrán,[1] J. Andrés,[1,*] J. A. Varela,[3] and E. Longo[3]
[1]*Departament de Química Física i Analítica, Universitat Jaume I, Campus de Riu Sec, Castelló E-12080, Spain*
[2]*LIEC, Departamento de Química, Universidade Federal de São Carlos-UFSCAR, P.O. Box 676, São Carlos, São Paulo 13565-905, Brazil*
[3]*LIEC, Instituto de Química, UNESP, P.O. Box 355, Araraquara, São Paulo 14801-907, Brazil*
(Received 20 May 2007; revised manuscript received 17 October 2007; published 14 February 2008)

Intercalation processes and corresponding diffusion paths of Li ions into spinel-type structured $Li_{1+x}Ti_2O_4$ ($0 \leqslant x \leqslant 0.375$) are systematically studied by means of periodic density functional theory calculations for different compositions and arrangements. An analysis of the site preference for intercalation processes is carried out, while energy barriers for the diffusion paths have been computed in detail. Our results indicate that the Li insertion is thermodynamically favorable at octahedral sites 16*c* in the studied composition range, and Li migration from tetrahedral sites 8*a* to octahedral sites 16*c* stabilizes the structure and becomes favorable for compositions $x \geqslant 0.25$. Diffusion paths from less stable arrangements involving Li migrations between tetrahedral and octahedral sites exhibit the lowest energy barrier since the corresponding trajectories and energy profiles take place across a triangle made by three neighboring oxygen anions without structural modification. Theoretical and experimental diffusion coefficients are in reasonable agreement.

DOI: 10.1103/PhysRevB.77.085112 PACS number(s): 71.15.Mb

I. INTRODUCTION

In recent years, spinel-type structured lithium titanium oxides have been subject of a large number of publications because of their promising applications as anodes in solid-state high energy Li ion batteries.[1–4] In particular, the Li-Ti-O spinel oxide studies are restricted in the composition range by two limiting compounds: $LiTi_2O_4$ and $Li_4Ti_5O_{12}$,[5,6] originally synthesized and characterized as end members in the solid solution system $Li_{1+y}Ti_{2-y}O_4$ ($0 \leqslant y \leqslant 1/3$).[7] These materials present good reversibility of the lithium insertion and/or extraction process without significant changes in cell volume (less than 2%) and show good capacity retention.[5,8–10] The combination of high lithium mobility and zero strain insertion properties[9,11,12] makes it an adequate anode for high rate battery applications. In addition, the fact that cells of Li-Ti-O spinel oxides produce no metallic lithium during charge makes them more attractive from a safety viewpoint compared to lithium cells that employ lithium-carbon anodes.[8]

The use of spinel $LiTi_2O_4$ as electrode material is based on its ability to host an additional amount of Li leading to composition $Li_2Ti_2O_4$.[13] The insertion capacity of the $LiTi_2O_4$ spinel toward Li addition was first reported by Murphy and co-workers in the early 1980s.[13,14] Colbow *et al.* cycled this material between about 3 and 1 V, leading to compositions between $x=-0.2$ and 1 for $Li_{1+x}Ti_2O_4$; for values of x between 0 and 1, the potential is constant around 1.34 V vs Li/Li^+, and Li can be reversible cycled with little capacity loss.[5] Furthermore, much attention has been paid to the composition of $LiTi_2O_4$, which was the first discovered superconducting oxide system having a transition temperature $T_c=11$ K.[6,15]

These materials are attractive enough not only to be used for the practical purposes but also to be employed as a model material in the fundamental study on solid-state electrochemical reactions. Experimental results offer extensive information that is yet to be explored, but they cannot probe directly the atomistic features of crystal and electronic structure along the intercalation processes and diffusion paths. Theory can complement these efforts and first-principles calculations are claimed to disclose a valuable complementary tool to help for understanding and providing insights into the relationship between the lithium composition and the nature of lithium intercalation and diffusion processes.

Several computational studies on $Li_{1+x}Ti_2O_4$ ($0 \leqslant x \leqslant 1$) ($Fd\bar{3}m$) spinel structure have been reported;[16,17] however, to the best of our knowledge, no theoretical analysis of Li diffusion has been reported until now. In this paper, we analyze, by means of numerical simulations, the thermodynamic and electronic properties of $Li_{1+x}Ti_2O_4$ system ($0 \leqslant x \leqslant 0.375$); in addition, since both fourfold and sixfold vacancies are presented in this structure, we have also investigated all possible Li intercalation processes and corresponding diffusion paths at different Li compositions and arrangements.

The remainder of the paper is organized as follows. Section II addresses the computing methods and model systems. In Sec. III A, we focus in the intercalation processes, giving values for their formation energies. Section III B is divided in three sections in which we describe and analyze the mechanisms of the diffusion paths at different compositions (Secs. III B 1 and III B 2), while the corresponding jump diffusion coefficients are reported in Sec. III B 3. Finally, we summarize our main conclusions in Sec. IV.

II. COMPUTING METHODS AND MODEL SYSTEMS

First-principles total energy calculations were carried out within the periodic density functional theory framework using the VASP program.[18,19] The Kohn-Sham equations have been solved by means of the generalized gradient approxi-

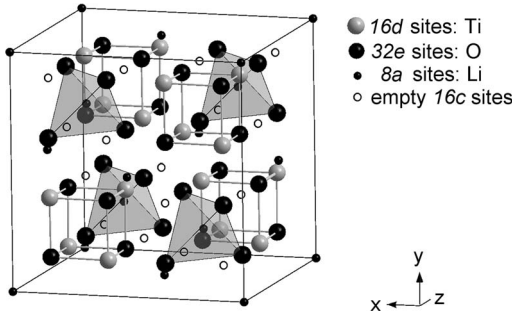

FIG. 1. Schematic figure of $LiTi_2O_4$ spinel structure.

mation (GGA) proposed by Perdew and Wang,[20,21] and the electron-ion interaction described by the projector augmented wave pseudopotentials.[22] The plane-wave expansion was truncated at cut off energy of 400 eV, and the Brillouin zones have been sampled through a Monkhorst-Pack $4\times4\times4$ k-point mesh until the forces on all atoms were less than 0.03 eV/Å assuring geometrical and energetic convergence for the $Li_{1+x}Ti_2O_4$ structures considered in this work. All the crystal structures are optimized in both simultaneously the volume of the cell and the atom positions. A spin-unrestricted approach (ISPIN option) has been employed when Li were inserted and migrated into the lattice. This methodology has been used in other recent works involving Li mobility on layered lithium transition metal oxides,[23] olivine $LiFePO_4$,[24,25] spinel $Li_xMn_2O_4$,[26] lithium halides,[27] TiO_2,[28,29] and WO_3,[30] as well as in diffusion studies of metal subsurface impurities.[31,32] Therefore, we are confident with the data calculated at this computing level for this type of processes.

$LiTi_2O_4$ spinel is characterized by a close cubic packing (space group $Fd\bar{3}m$) with eight $LiTi_2O_4$ units per unit cell, in which lithium ions are located at 8a tetrahedral sites, titanium ions at 16d octahedral sites, and oxide ions at 32e sites. Since this unit cell has 64 tetrahedral and 32 octahedral holes, there are 56 empty tetrahedra and 16 empty octahedral sites. The unit cell can be partitioned into five types of polyhedra that fill completely its volume: TiO_6 octahedra, LiO_4 tetrahedra, O_6 octahedra, $(O_4)1$, and $(O_4)2$ tetrahedra, with multiplicities of 16, 8, 16, 8, and 48, respectively. Figure 1 outlines the unit cell of $LiTi_2O_4$ showing the occupied 8a, 16d, and 32e sites and the empty 16c octahedral sites. Intercalation processes were considered by placing Li ions in these empty 16c octahedral sites during electrochemical reactions in the $Li_{1+x}Ti_2O_4$ ($0\leqslant x\leqslant 1$) systems, while alternative diffusion paths of the Li ions from the occupied 8a tetrahedral sites to the empty 16c octahedral sites were analyzed. The optimization procedure takes into account the atomic positions of the first and second nearest neighbors of the jumping Li ions during the migration processes. Similar diffusion channels have been considered previously for $Li_xMn_2O_4$ spinel systems, in which the lithium intersite hopping between 8a and 16c sites is presumably the primary lithium conduction process.[33]

The energy associated with intercalation processes E_{int} of Li ions in a $LiTi_2O_4$ bulk was calculated by the following equation:

$$E_{int} = E_{\mathrm{Li}+bulk} - nE_{\mathrm{Li}} - E_{bulk}, \quad (1)$$

where $E_{\mathrm{Li}+bulk}$ is the binding energy of the $Li_{1+x}Ti_2O_4$ system, n is the number of intercalated Li, E_{Li} is the thermodynamic chemical potential of a lithium, and E_{bulk} is the binding energy of the bulk $LiTi_2O_4$. The reference chemical potential of lithium can be calculated in several ways,[34] although is often referred to the solid Li. One can also relate it to the Li atom in the ground state, and in the present study, E_{Li} is calculated by placing one Li in a large cell with the same lattice parameters of the host crystal (a=8.363 Å).

The diffusion coefficient of Li ion in electrode materials is a key parameter of the rate capability of rechargeable Li batteries and it depends on several factors. Li hopping requires at least an adjacent vacancy to hop into, and Li ion will have more possibilities to migrate if it is surrounded by many vacancies. This depends on the overall lithium concentration and the equilibrium degree at short or long range. The jump diffusion coefficient D_J for lithium hopping to vacant neighboring sites has the form $D_J=\Gamma l^2$; l and Γ are the hopping distance and rate, respectively. Here, Γ can be estimated by the activation barriers of the migration process as[35]

$$\Gamma = \nu_0 \exp(-\Delta E/K_B T), \quad (2)$$

where ν_0 is the vibrational frequency of a migrating specie around its equilibrium position that is typically on the order 10^{13} s^{-1} (value used in this work) and ΔE is the mean jump activation energy, i.e., the difference in energy at the activated state and the energy at the initial equilibrium state of the hop. The activated state is located at the maximum energy point along the minimum energy path between the end points of the hop.

III. RESULTS AND DISCUSSION

A. Intercalation processes

First, we have carried out a detailed study on the intercalation processes of 1, 2, and 3 Li ions into the unit cell of the structure $Li_{1+x}Ti_2O_4$ ($0\leqslant x\leqslant 0.375$), resulting Li concentrations of x=0.125, 0.250, and 0.375, respectively. Different configurations were calculated corresponding to different 8a/16c ratios. The selected nomenclature was T-O, where T and O denote the numbers of Li ion located at tetrahedral (8a) and octahedral (16c) sites, respectively. Table I presents the values of both total and relative energies per unit cell of the spinel-type $Li_{1+x}Ti_2O_4$ ($0\leqslant x\leqslant 0.375$) for the most stable arrangements of different configurations at each value of Li concentration x. It is important to remark that lithium can be inserted and extracted without significant changes of lattice dimensions. Then, the intercalation process provides a volume change of less than 1% as the Li concentration is increased.

The structure $LiTi_2O_4$, x=0, is labeled as configuration 8-0 and it presents all the Li located in 8a tetrahedral sites and has all 16c octahedral sites empty. In the configuration 7-1, seven Li ions remain in 8a sites and one Li ion is located in 16c site; in principle, there are 8 possibilities for 8a sites and 16 for 16c sites, but only 3 arrangements are nonequivalent. The most stable arrangement for this 7-1 configu-

TABLE I. Values of total and relative energies per $Li_{1+x}Ti_2O_4$ unit cell of the most stable arrangements from different configurations.

	Configuration	Energy (eV)	ΔE (eV)
$LiTi_2O_4$	8-0	−458.350	0.00
	7-1	−456.803	1.55
	6-2	−456.343	2.01
$Li_{1.125}Ti_2O_4$	8-1	−459.989	0.00
	7-2	−459.515	0.47
	6-3	−459.077	0.91
$Li_{1.250}Ti_2O_4$	8-2	−461.630	0.00
	7-3	−462.092	−0.46
	6-4	−461.612	0.02
$Li_{1.375}Ti_2O_4$	8-3	−463.335	0.00
	7-4	−464.503	−1.17

ration is depicted in Fig. 2(a), being 1.55 eV less stable than the configuration 8-0, as presented in Table I. The configuration 6-2 presents four nonequivalent arrangements, and the most stable of them is shown in Fig. 2(b). This arrangement is 2.01 eV less stable than configuration 8-0.

At composition $x=0.125$, $Li_{1.125}Ti_2O_4$, the most stable arrangement of the 8-1 configuration is depicted in Fig. 2(c), while the most stable arrangements for the configurations 7-2 [see Fig. 2(d)] and 6-3 [see Fig. 2(e)] present values of relative energies with respect 8-1 of 0.47 and 0.91 eV, respectively.

In model $Li_{1.250}Ti_2O_4$, $x=0.250$, the different arrangements for both configurations 8-2 and 7-3 as well as the diagram of relative energies are illustrated in Figs. 3 and 4, respectively. The three nonequivalent arrangements for the configuration 8-2 are depicted in Fig. 3(a) and the stability order is $E1_{8\text{-}2}<E2_{8\text{-}2}<E3_{8\text{-}2}$, where the type of configuration is referred as subscript. The most stable arrangement of the configuration 7-3 is shown as E1 ($E1_{7\text{-}3}$) in Fig. 3(b), together with the 19 possible local Li arrangements of this configuration. An analysis of the results points out that $E1_{8\text{-}2}$ is less stable than $E1_{7\text{-}3}$ by 0.46 eV, while the most favorable arrangement of the configuration 6-4 [illustrated in Fig. 3(c)] is slightly less stable than the $E1_{8\text{-}2}$ by 0.02 eV (see Table I).

For composition $x=0.375$, the values of the relative energies for the different arrangements of the configurations 8-3 and 7-4 are listed in Figs. 5(a) and 5(b), respectively. In contrast with the results reported for $x=0.250$ (see Fig. 4), four arrangements of configuration 7-4 are clearly more stable than the corresponding to 8-3 configuration.

A global analysis of the results reported in Table I and Fig. 2–5 shows that for a given value of x, the lithium diffusion processes from 8*a* tetrahedral to 16*c* octahedral sites will be thermodynamically favorable only in the composition range of $x=0.250$ and 0.375, i.e., 7-3 and 7-4 are more stable than 8-2 and 8-3 configurations, respectively. Table II gives the values of intercalation energies per $Li_{1+x}Ti_2O_4$ unit cell of the most stable arrangements from different configurations, providing values in a range between −1.3 and −6.9 eV. When eight Li ions remain in 8*a* sites, each lithium intercalated in the vacant 16*c* site contributes with a gain of stability of ≃1.4 eV. However, when seven or six Li ions are maintained in 8*a* sites and one or two Li ions are located in empty 16*c* sites, respectively, each inserted lithium supplies an energy gain of ≃2.4 eV in the resulting structure. These results indicate that lithium intercalation processes appear to be thermodynamically favorable in all studied range of composition. This increase of stability in intercalation processes when 8*a* sites are not totally occupied points out that the diffusion processes from tetrahedral 8*a* sites to octahedral 16*c* sites are also energetically favorable from a thermodynamic point of view.

B. Diffusion paths

At a particular value of x, different Li diffusion paths in the structure $Li_{1+x}Ti_2O_4$ can be theoretically investigated in order to find energetically favorable channels from a thermodynamic and kinetic point of view. In agreement with previous results obtained for intercalation processes, diffusion paths were analyzed at compositions $x=0.250$ and 0.375. Four sets for the diffusion channel have been considered, namely:

(1) Li migrations from 8*a* to 16*c* sites involving the most stable Li arrangements for each configuration. Therefore, at $x=0.250$, a Li diffusion path from arrangements $E1_{8\text{-}2}$ and $E1_{7\text{-}3}$ has been considered, hereafter called path 1; for x

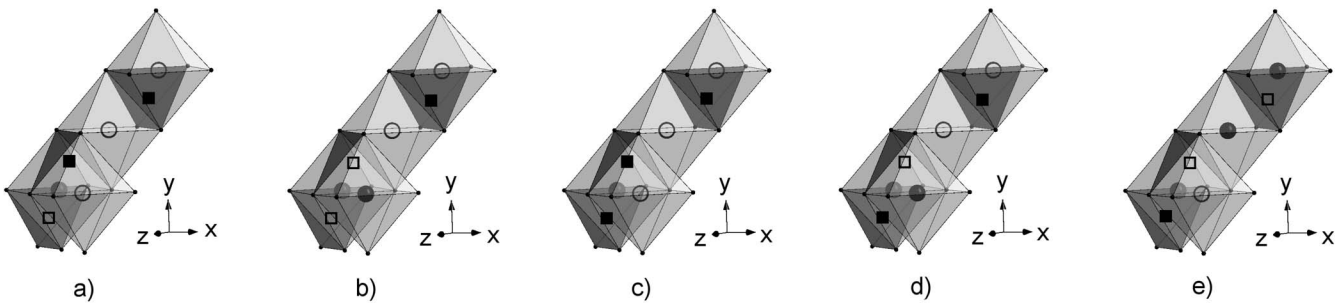

FIG. 2. The most stable local Li arrangements of the configurations (a) 7-1, (b) 6-2, (c) 8-1, (d) 7-2, and (e) 6-3. The circles are 16*c* octahedral sites and the squares are 8*a* tetrahedral sites. The black circles and black squares are filled sites by Li, while the gray circles and gray squares are empty sites.

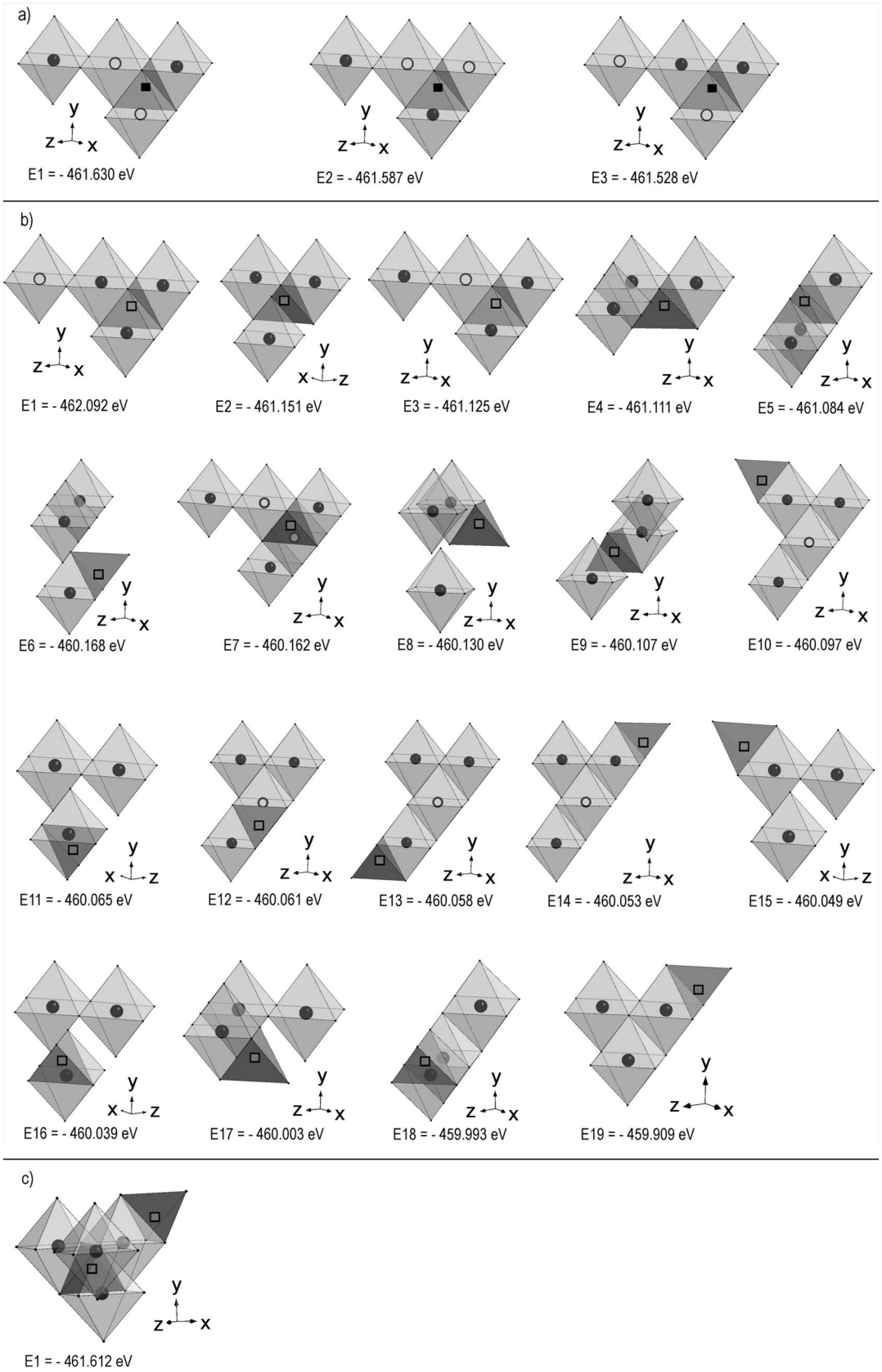

FIG. 3. (a) Local Li arrangements of the configuration 8-2, (b) local Li arrangements of the configuration 7-3, and (c) the most stable arrangement of the configuration 6-4 in the $Li_{1.250}Ti_2O_4$ structure. The circles are 16*c* octahedral sites and the squares are 8*a* tetrahedral sites. The black circles and black squares are filled sites by Li, while the gray circles and gray squares are empty sites. Values of the total energies per $Li_{1.250}Ti_2O_4$ unit cell are presented.

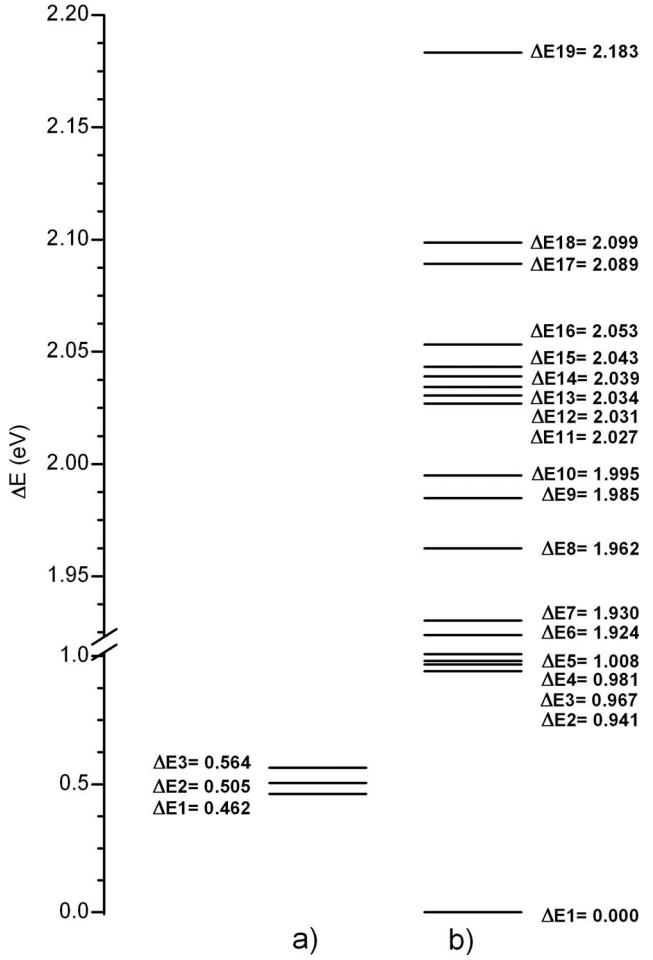

FIG. 4. Diagram of relative energy values per $Li_{1.250}Ti_2O_4$ unit cell containing nonequivalent Li arrangements of the configurations (a) 8-2 and (b) 7-3. Energy differences with regard to the arrangement $E1_{7\text{-}3}$ (−462.092 eV).

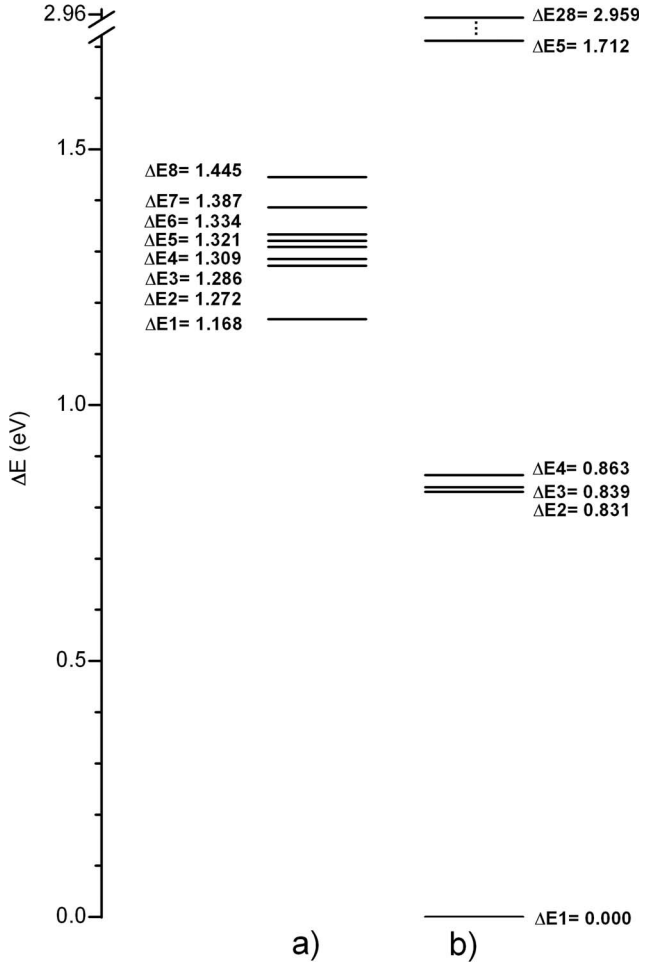

FIG. 5. Diagram of relative energy values per $Li_{1.375}Ti_2O_4$ unit cell containing nonequivalent Li arrangements of the configurations (a) 8-3 and (b) 7-4. Energy differences with regard to the arrangement $E1_{7\text{-}4}$ (−464.503 eV).

=0.375, the analysis is carried out for the path that connects $E1_{8\text{-}3}$ to $E1_{7\text{-}4}$.

Assuming that a wide range of different Li arrangements is formed during the Li insertion process due to internal tensions caused by voltage application, we can also consider Li migrations from 8*a* sites to 16*c* sites involving less stable Li arrangements. Therefore, the investigation of different Li diffusion paths involving less stable configurations can be classified in the next sets:

(2) Li diffusion path from the $E1_{8\text{-}3}$ to $E3_{7\text{-}4}$ arrangements, called path 2, at $x=0.375$.

(3) Li diffusion paths from the arrangements $E2_{8\text{-}2}$ and $E3_{8\text{-}2}$ as starting points to reach $E1_{7\text{-}3}$, called paths 3.1 and 3.2, respectively, for $x=0.250$. For $x=0.375$, path 3.3 corresponds to Li migration from $E8_{8\text{-}3}$ to $E1_{7\text{-}4}$.

(4) Li diffusion path from $E4_{8\text{-}3}$ to $E2_{7\text{-}4}$ arrangements, called path 4, at $x=0.375$.

1. At composition x=0.250

The results obtained for path 1 of set (1) are depicted in Fig. 6. The Li ion to be migrated can be located at both 8*a* and 16*c* sites. Therefore, three alternative diffusion channels can be delineated. (i) Path 1a where Li migration involves the shift of a Li ion from one 8*a* site to one 16*c* site to obtain $E3_{7\text{-}3}$; from this arrangement, one Li can be displaced from another 16*c* site to an adjacent 16*c* site. (ii) Path 1b where Li migrates between adjacent 16*c* sites to yield $E3_{8\text{-}2}$, and then other Li located at 8*a* site shifts to one 16*c* site. (iii) Path 1c which involves the concerted diffusion of the previous four Li migrations from $E1_{8\text{-}2}$ to $E1_{7\text{-}3}$ arrangements. The corre-

TABLE II. Values of intercalation energies per $Li_{1+x}Ti_2O_4$ unit cell of the most stable arrangements of different configurations, calculated by Eq. (1). The value of energy for one Li is −0.274 eV.

	$LiTi_2O_4$	$Li_{1.125}Ti_2O_4$	$Li_{1.250}Ti_2O_4$	$Li_{1.375}Ti_2O_4$
Configuration	8-0	8-1	8-2	8-3
E_{int} (eV)	0.00	−1.37	−2.73	−4.16
Configuration	7-1	7-2	7-3	7-4
E_{int} (eV)	0.00	−2.44	−4.74	−6.88
Configuration	6-2	6-3	6-4	
E_{int} (eV)	0.00	−2.46	−4.72	

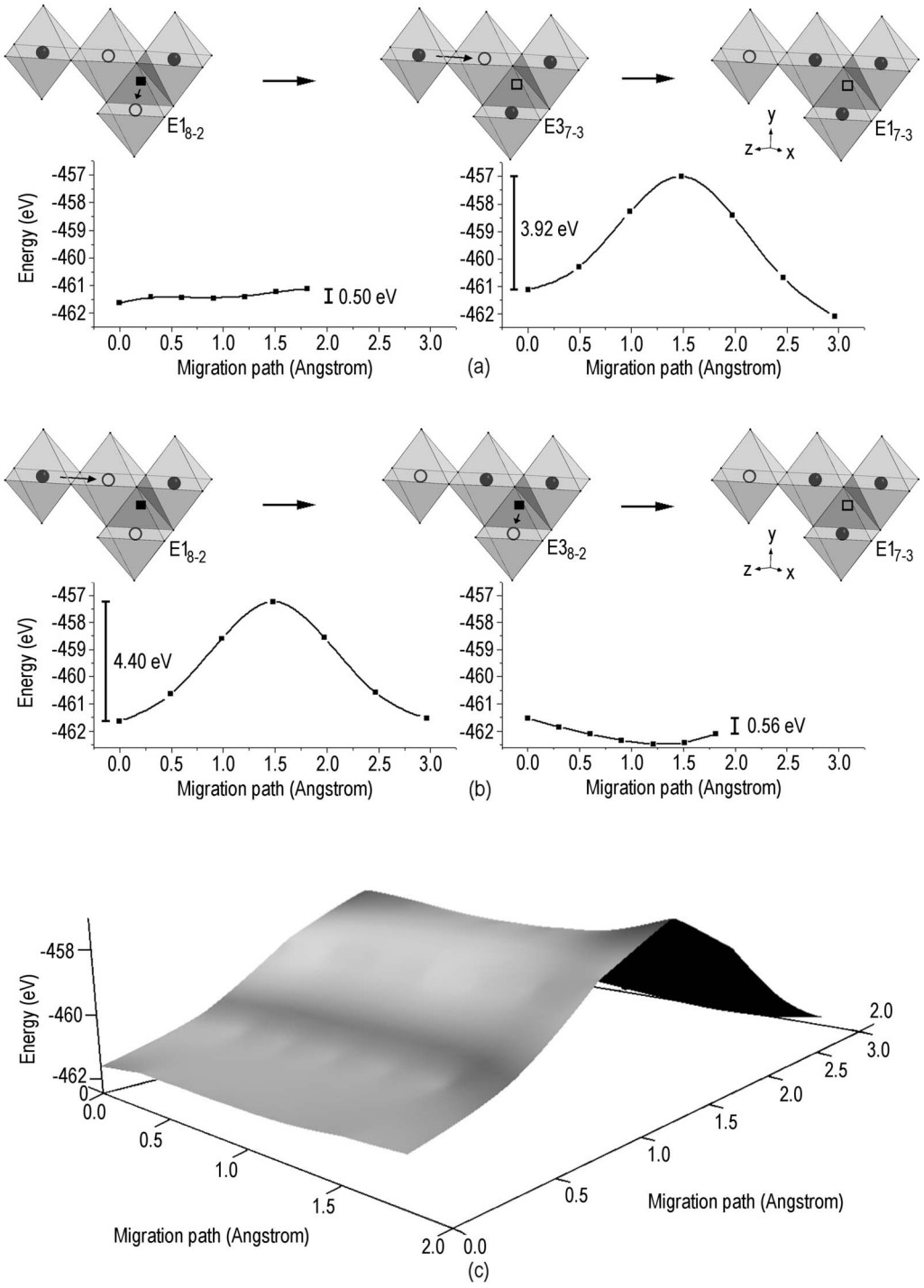

FIG. 6. Energy profiles for Li diffusion paths belonging to set (1) for x=0.250: (a) path 1a involving two Li migrations from E1$_{8-2}$ to E1$_{7-3}$; (b) path 1b implying two Li migrations from E1$_{8-2}$ to E1$_{7-3}$; (c) simultaneous path 1c.

sponding energy profiles, energy vs hoping distance, for both paths 1a and 1b are presented in Figs. 6(a)–6(c), respectively, while a tridimensional surface of path 1c is depicted in Fig. 6(c).

An analysis of the results shows that the first stage of path 1a is associated with a continuous increase of the energy from E1$_{8-2}$ to E3$_{7-3}$, 0.50 eV; while the second step presents a high barrier of 3.92 eV at 1.5 Å. These energetic values corresponding to the different migrations can be associated with the Li overlapping with neighboring oxygen anions along its motion toward the vacant site. Therefore, the key role of oxide ions along the electronic exchange during the migration processes has been analyzed. In the first stage of path 1a, Li hopes from the 8*a* to the 16*c* site and this channel takes place across the center of a triangle made by three neighboring oxygen anions without significant structural modifications; as a result, this path presents a lower barrier height. However, in the second step of path 1a, Li moves

between adjacent 16*c* sites implying the direct pass through two oxygen anions which undergo an increase of their negative charge to ≈6.5%; thus, at the maximum in the energy profile, a large value of electronic charge from the migrating Li is transferred to them. In addition, from a structural point of view, a noticeable enlargement of the distance between these two oxygen anions takes place from 3.07 to 3.28 Å. Then, the value of energy barrier of the diffusion path increases on going from the first to the second stage of path 1a. These remarks are similar to those employed in the Li mobility in Li_xCoO_2 by Van der Ven *et al.*[36] and lithium halides by Kishida *et al.*[27] Path 1b presents an opposite trend with regards to path 1a: the first stage presents a barrier height of 4.40 eV and the jumping Li ion overlaps significantly with neighboring oxygen counterions while it passes through, resulting in a significant energy barrier. This structural hindrance is avoided along the second stage since Li ion moves through the center of the triangle made by the three neighboring oxygen anions. Path 1c takes place via a maximum, located at 1.2 and 1.5 Å, with a relative energy with respect $E1_{8\text{-}2}$ of 3.84 eV.

As can be seen in Fig. 4, the $Li_{1.250}Ti_2O_4$ structure has only one arrangement of the configuration 7-3 ($E1_{7\text{-}3}$) more stable than the arrangements of the configuration 8-2. The investigation of Li diffusion processes of set (3) involving less stable arrangements as starting points, $E2_{8\text{-}2}$ and $E3_{8\text{-}2}$, to reach the final most stable arrangement, $E1_{7\text{-}3}$, is carried out by the study of paths 3.1 and 3.2, respectively. The migration paths from $E2_{8\text{-}2}$ to $E1_{7\text{-}3}$ were also analyzed in three different forms. (i) Path 3.1a, where one Li migrates from one 8*a* site to one 16*c* site to reach $E3_{7\text{-}3}$, and then a different Li ion shifts between 16*c* sites, achieving the arrangement $E1_{7\text{-}3}$. (ii) Path 3.1b, where Li migrates between 16*c* sites, and then another Li moves from one 8*a* site to one 16*c* site also reaching the arrangement $E1_{7\text{-}3}$. (iii) Path 3.1c, which implies the simultaneous diffusion of the previous four Li migrations from $E2_{8\text{-}2}$ to $E1_{7\text{-}3}$. An analysis of the corresponding energy profiles for both paths 3.1a and 3.1b presented in Figs. 7(a) and 7(b), respectively, shows an increase of the energy from $E2_{8\text{-}2}$ to $E3_{7\text{-}3}$ of 0.46 eV in the first stage of path 3.1a and a high barrier of 3.92 eV associated with the second stage; however, for path 3.1b, the first stage implies the overcoming of an energy barrier of 3.98 eV and in the second one, the achievement of the arrangement $E1_{7\text{-}3}$ along a barrierless process. Finally, in Fig. 7(c), a tridimensional representation for path 3.1c is depicted, where concerted Li migration processes involve a barrier height of 3.77 eV with respect $E2_{8\text{-}2}$, and this maximum is located at 1.3 and 1.5 Å. Path 3.2 from $E3_{8\text{-}2}$ to $E1_{7\text{-}3}$ classified inside set (3) only involves one migration process between 8*a* and 16*c* sites without energy barrier. This path has been previously described in Fig. 6(b) and can be envisioned as the second segment of path 1b.

2. At composition $x=0.375$

For $x=0.375$, four arrangements belonging to configuration 7-4 are more stable than eight of the configuration 8-3 (see Fig. 5), and consequently, there are several possibilities of Li diffusion paths between both configurations. Therefore, we have selected for each set of diffusion processes, (1)–(4), the corresponding path that involves a minor number of Li migrations between the different sites of the $Li_{1.375}Ti_2O_4$ structure.

The diffusion path belonging to set (1) implies the Li migration from the arrangement $E1_{8\text{-}3}$ to the $E1_{7\text{-}4}$. This channel involves at least three migration processes, namely, two migrations between 16*c* sites and one migration between 8*a* and 16*c* sites. The energy profile depicted in Fig. 8 is associated with a Li migration process between 16*c* sites, which presents a large value for the energy barrier, 4.22 eV. Therefore, the subsequent steps have not been considered.

The diffusion path of set (2) at $x=0.375$, related to the Li mobility from $E1_{8\text{-}3}$ to $E3_{7\text{-}4}$ arrangements, involves at least three migration processes between 8*a* and 16*c* sites. This path, called path 2, was investigated by two different ways and is depicted in Fig. 9(a). The first one, path 2a, is a stepwise involving three consecutive processes: (i) the Li hoping between Tet1 (black square) and Oct4 (white circle), (ii) the Li migration between Tet2 (black square) and Oct5 (white circle), and (iii) the Li migration between Oct1 (black circle) and Tet2 (black square). The second one corresponds to a concerted movement of the Li ions along the three different migrations above mentioned, path 2b. The energy profile for both path 2a (black square points) and path 2b (white square points) is presented in Fig. 9(b). In the first step of path 2a, one Li migrates from the tetrahedral site Tet1 to the octahedral site Oct4 through the points 1, 2, 3, 4, and 5. In the second step, one Li migrates from the tetrahedral site Tet2 to the octahedral site Oct5 through the points 1′, 2′, 3′, 4′, and 5′. In the third step, one Li migrates from the octahedral site Oct1 to the tetrahedral site Tet2 through the points 1″, 2″, 3″, 4″, and 5″. The continuous path 2b of set (2) can be described in the following way. First, Li from sites Tet1, Tet2, and Oct1 migrate simultaneously to the points 1, 1′, and 1″, respectively. Second, one Li from points 1, 1′, and 1″ migrate simultaneously to the points 2, 2′, and 2″ and thus successively until to reach the arrangement $E3_{7\text{-}4}$. This continuous path 2b presents an overall barrier height of 0.48 eV, lower than the barrier of path 2a (0.54 eV) and also is more realistic because the repulsive forces act on the three Li at the same time. These paths resulted in a lower energy barrier when compared with the barrier of 4.22 eV from one path segment of set (1) involving Li migration between octahedral sites (Fig. 8).

In Fig. 10(a), one diffusion path belonging to set (3) for $x=0.375$ is illustrated, where one Li migrates from the arrangement $E8_{8\text{-}3}$ to the arrangement $E1_{7\text{-}4}$. This path 3.3 only involves one migration process between 8*a* and 16*c* sites, and its energy profile graph shows the Li migration to the more stable (1.44 eV) arrangement $E1_{7\text{-}4}$ without energy barrier. The diffusion path of set (4) at $x=0.375$ is presented in Fig. 10(b). It has been studied the Li mobility along path 4 from $E4_{8\text{-}3}$ to $E2_{7\text{-}4}$, which only involves one migration between 8*a* and 16*c* sites. As depicted in Fig. 10(b), Li in 8*a* site (square) migrates to a 16*c* site (circle) reaching a more stable (0.48 eV) arrangement $E2_{7\text{-}4}$ without potential barrier. This path can also be classified as a Li migration path segment of set (1) because it is a continuity of the path from Fig. 8.

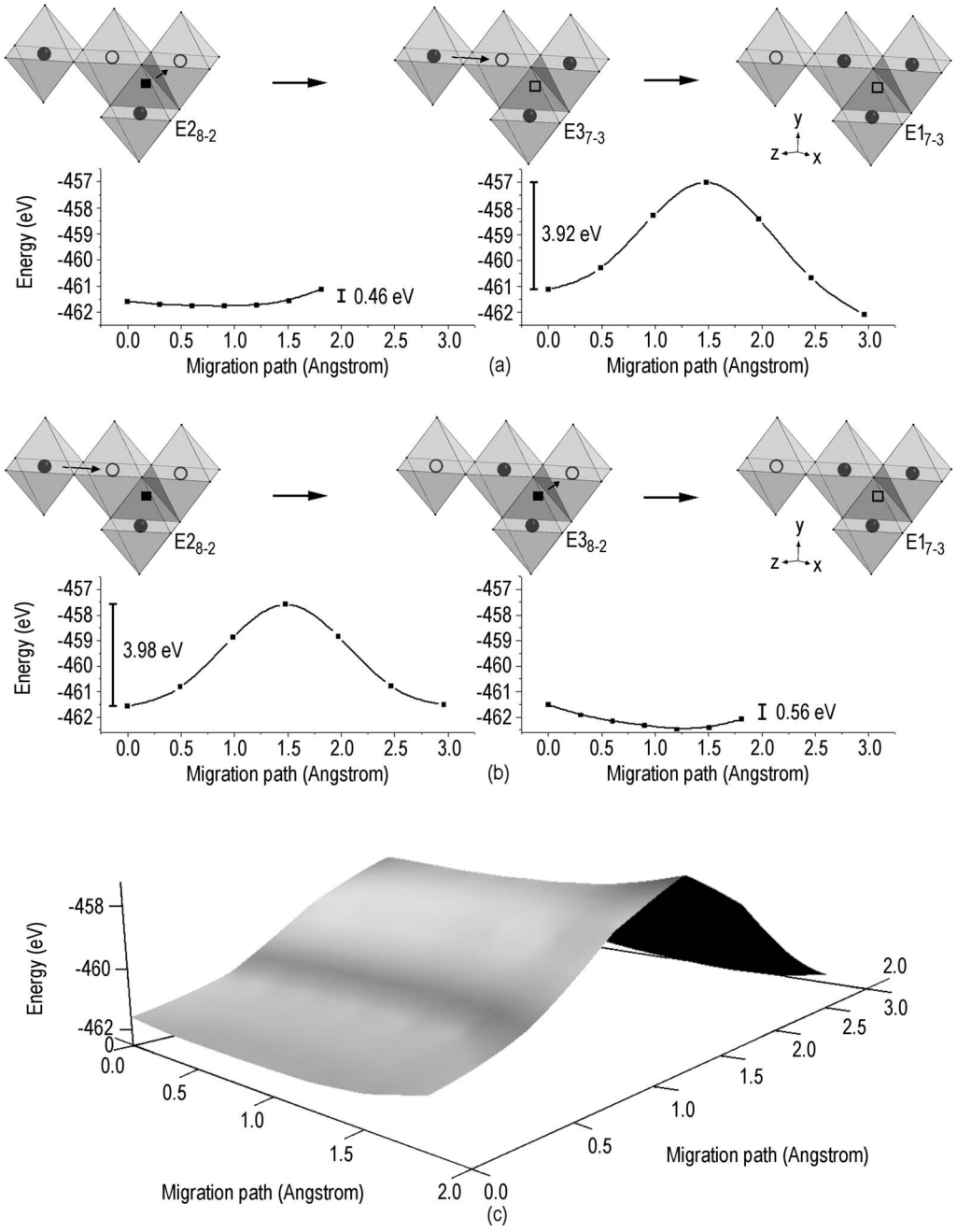

FIG. 7. Energy profiles for Li diffusion paths belonging to set (3) for $x=0.250$: (a) path 3.1a involving two Li migrations from E2$_{8-2}$ to E1$_{7-3}$; (b) path 3.1b implying two Li migrations from E2$_{8-2}$ to E1$_{7-3}$; (c) simultaneous path 3.1c.

3. Jump diffusion coefficient

It is interesting to elucidate the variation of the hopping barrier and the jump diffusion coefficient with composition, along the different diffusion paths found between each configuration. Since the hop frequency Γ is proportional to the exponential of the activation barrier, the jump diffusion coefficient D_J can be easily obtained taking into account the hopping distance. For composition $x=0.250$, the simultaneous path 1c from E1$_{8-2}$ to E1$_{7-3}$ [set (1)] involves a barrier height of 3.84 eV, whereas a minimum value of 3.77 eV is obtained for the simultaneous path 3c starting from E2$_{8-2}$ [set (3)]. The D_J for both is in order of $\sim 10^{-19}$ cm^2 s^{-1} (900 °C). For composition $x=0.375$, one segment of the Li migration corresponding to set (1) involves a potential barrier of 4.22 eV, which is a D_J similar to previous composition. Nevertheless, the concerted path 2b corresponding to set (2) described in Fig. 9 has a lower potential barrier of 0.48 eV, which results in a $D_J=2.8\times 10^{-5}$ cm^2 s^{-1} for a hopping distance $l=1.81$ Å (900 °C). To our knowledge, there are only two diffusion experiments of lithium ion in Li-Ti-O spinel oxides. One of them, using neutron radiography, obtained values of the jump diffusion coefficient in the range of $(1.3-2.2)\times 10^{-6}$ cm^2 s^{-1} at 860, 880, and 900 °C, respectively, for the $Li_{1.33}Ti_{1.67}O_4$ structure.[37] Recently, a second

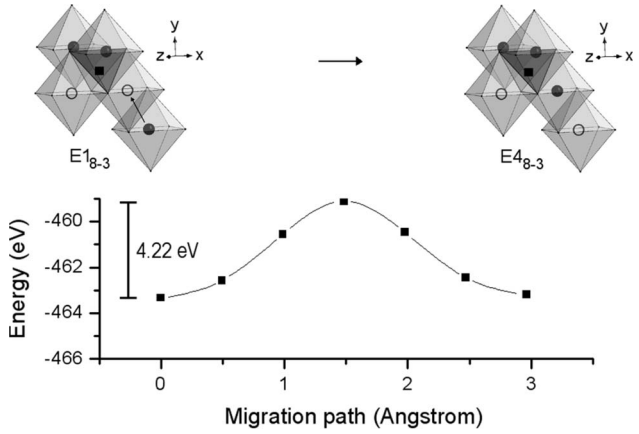

FIG. 8. Energy profile for a Li diffusion path segment of set (1) for $x=0.375$ involving a Li migration process from E1$_{8-3}$ to E4$_{8-3}$.

study for the same structure reported a jump rate value of 4.9×10^{8} s^{-1} above 420 K by means of NMR and impedance spectroscopy.[38] These reported studies can be interpreted as a resulting measure of the total migration possibilities compared to our theoretical results, which can be understood as upper bounds. A comparison to the similar $Li_xMn_2O_4$ spinel can be performed since reported data using one-dimensional NMR spectral intensities[33] have determined activation energies for jumping Li from 8*a* to 16*c* sites and vice versa; their value of 0.5 eV for the activation energy is in good agreement with the value found in this study, and they reported D_J values of 10×10^{-16} cm^2 s^{-1} for a hopping distance $l=1.78$ Å, although at a range of temperature between 300 and 400 K.

IV. CONCLUSIONS

In this study, the ability of $Li_{1+x}Ti_2O_4$ spinel structure to be used as electrode material was investigated by means of first-principles calculations based on the density functional theory under the GGA approximation. The results presented have strong implications toward improved intercalation and diffusion processes in spinel-type structured $Li_{1+x}Ti_2O_4$ ($0\leqslant x\leqslant0.375$), which forms the basis of a number of solid-state electrochemical applications and needs to a deep theoretical comprehension in order to identify the more favorable stages of the diffusion process during the Li insertion and/or extraction. The different arrangements for each studied composition have been characterized in depth, and energy profiles for Li migration paths as well as the corresponding jump diffusion coefficients have been reported. The main results can be summarized as follows.

(i) Calculations predict that the $Li_{1+x}Ti_2O_4$ spinel becomes more stable after the Li intercalation process in 16*c* sites for all range studied of *x*, whereas Li diffusion pro-

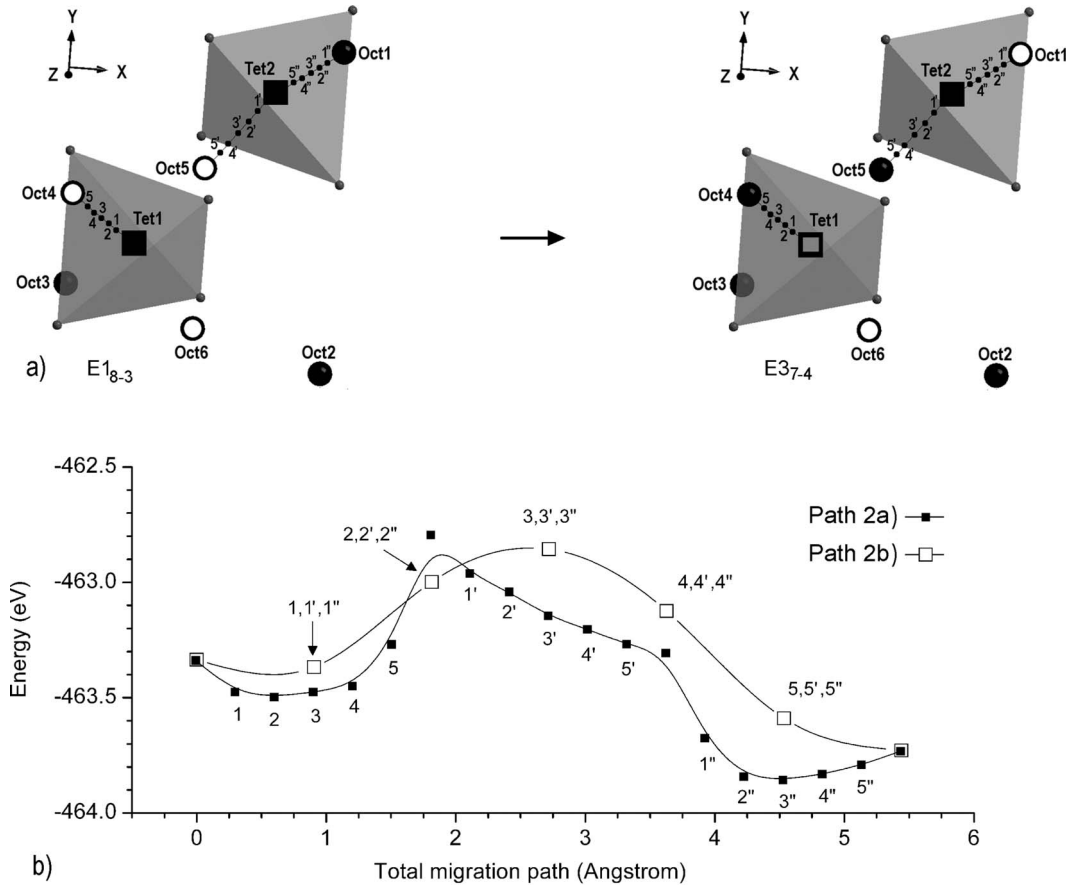

FIG. 9. (a) Li diffusion paths belonging to set (2) for $x=0.375$, in which Li moves from E1$_{8-3}$ to E3$_{7-4}$ involving three Li migration processes between 8*a* and 16*c* sites. (b) Energy profiles for path 2a (black squares); path 2b continuous (white squares).

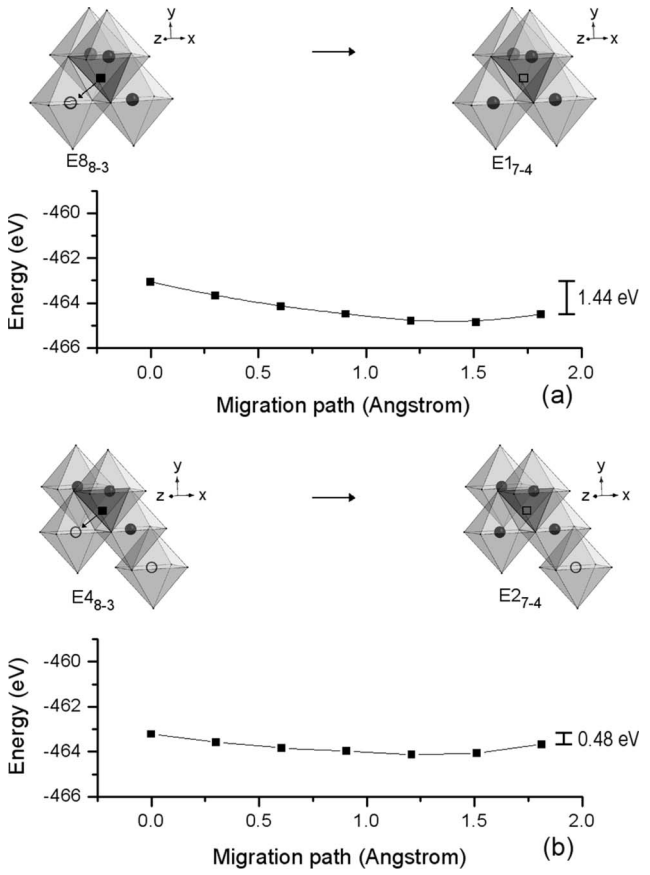

FIG. 10. Energy profiles for Li diffusion paths belonging to sets (3) and (4) for $x=0.375$: (a) path 3.3 belonging to set (3) involving one Li migration from E8$_{8-3}$ to E1$_{7-4}$; (b) path 4 belonging to set (4), which involves a Li migration from E4$_{8-3}$ to E2$_{7-4}$.

cesses from tetrahedral 8*a* sites to octahedral 16*c* sites are thermodynamically favorable only in the compositions $x \geqslant 0.250$.

(ii) The diffusion process from the most stable Li arrangement of a configuration to the most stable arrangement of another configuration involves at least one Li migration between 16*c* sites. The Li migrations between adjacent 16*c* sites present higher energy barriers ($\approx$4 eV) implying the direct pass through two oxygen anions which undergo an increase of their negative charge to $\simeq$6.5% as well as a noticeable enlargement of the distance between them at the maximum in the energy profile.

(iii) Lithium ions located in less stable Li local arrangements become free toward the 8*a*-16*c* diffusion with minor energetic cost than the lithium ions positioned in more stable arrangements, being the Li bindings stronger in more stable arrangements than in less stable arrangements. Therefore, the diffusion paths from less stable arrangements involving Li migrations between 8*a* and 16*c* sites are more favorable because the Li migrates without or with lower potential barriers ($\approx$0.5 eV), and the pass through the center of a triangle made by three neighboring oxygen anions takes place nearly without structural modification.

(iv) Path 3.2 from E3$_{8-2}$ to E1$_{7-3}$ for $x=0.250$ and path 3.3 from E8$_{8-3}$ to E1$_{7-4}$ and path 4 from E4$_{8-3}$ to E2$_{7-4}$ for $x=0.375$ only involve one migration process between 8*a* and 16*c* sites, being the most favorable diffusion pathways without overcoming potential barriers. In addition, the concerted path 2b has a lower potential barrier (0.48 eV) which results in a diffusion coefficient of 2.8×10^{-5} cm^2 s^{-1}.

ACKNOWLEDGMENTS

This work was partially supported by DGI (Project No. CT2006-15447-CO2-O1/BQU), by Generalitat Valenciana (Project No. ACOMP06/122), and Fundación Bancaixa-UJI (Projects Nos. P1 1B2005-20 and P1 1B2005-13). L. Gracia acknowledges support by the Postdoctoral grant (APOSTD07) from Generalitat Valenciana. M. Anicete-Santos also acknowledges the Brazilian agency CNPq.

*andres@qfa.uji.es

[1] J. M. Tarascon and M. Armand, Nature (London) **414**, 359 (2001).
[2] J. Thomas, Nat. Mater. **2**, 705 (2003).
[3] A. Hammami, N. Raymond, and M. Armand, Nature (London) **424**, 635 (2003).
[4] B. Scrosati, Nature (London) **373**, 557 (1995).
[5] K. M. Colbow, J. R. Dahn, and R. R. Haering, J. Power Sources **26**, 397 (1989).
[6] D. C. Johnston, H. Prakash, W. H. Zachariasen, and R. Viswanathan, Mater. Res. Bull. **8**, 777 (1973).
[7] A. Deschanvres, B. Raveau, and Z. Sekkal, Mater. Res. Bull. **6**, 699 (1971).
[8] E. Ferg, R. J. Gummow, A. Kock, and M. M. Thackeray, J. Electrochem. Soc. **141**, L147 (1994).
[9] T. Ohzuku, A. Ueda, and N. Yamamoto, J. Electrochem. Soc. **142**, 1431 (1995).
[10] D. Peramunage and K. M. Abraham, J. Electrochem. Soc. **145**, 2609 (1998).
[11] K. Ariyoshi, R. Yamato, and T. Ohzuku, Electrochim. Acta **51**, 1125 (2005).
[12] F. Ronci, P. Reale, B. Scrosati, S. Panero, V. R. Albertini, P. Perfetti, M. di Michiel, and J. M. Merino, J. Phys. Chem. B **106**, 3082 (2002).
[13] D. W. Murphy, M. Greenblatt, S. M. Zahurak, R. J. Cava, J. V. Waszczak, G. W. Hull, and R. S. Hutton, Rev. Chim. Miner. **19**, 441 (1982).
[14] R. J. Cava, D. W. Murphy, S. Zahurak, A. Santoro, and R. S. Roth, J. Solid State Chem. **53**, 64 (1984).
[15] D. C. Johnston, J. Low Temp. Phys. **25**, 145 (1976).
[16] Y. Takahashi, Y. Gotoh, and J. Akimoto, J. Phys. Chem. Solids **63**, 987 (2002).
[17] W. Y. Ra, M. Nakayama, Y. Uchimoto, and M. Wakihara, J. Phys. Chem. B **109**, 1130 (2005).
[18] G. Kresse and J. Hafner, Phys. Rev. B **49**, 14251 (1994).
[19] G. Kresse and J. Furthmuller, Comput. Mater. Sci. **6**, 15 (1996).

[20] J. P. Perdew, J. A. Chevary, S. H. Vosko, K. A. Jackson, M. R. Pederson, D. J. Singh, and C. Fiolhais, Phys. Rev. B **46**, 6671 (1992).
[21] J. P. Perdew and Y. Wang, Phys. Rev. B **45**, 13244 (1992).
[22] G. Kresse and D. Joubert, Phys. Rev. B **59**, 1758 (1999).
[23] K. Kang and G. Ceder, Phys. Rev. B **74**, 094105 (2006).
[24] Chuying Ou-Yang, Siqi Shi, Z. Wang, X. Huang, and L. Chen, Phys. Rev. B **69**, 104303 (2004).
[25] S. Miao, M. Kocher, P. Rez, B. Fultz, R. Yazami, and C. C. Ahn, J. Phys. Chem. A **111**, 4242 (2007).
[26] C. Y. Ouyang, S. Q. Shi, Z. X. Wang, H. Li, X. J. Huang, and L. Q. Chen, Europhys. Lett. **67**, 28 (2004).
[27] I. Kishida, Y. Koyama, A. Kuwabara, T. Yamamoto, F. Oba, and I. Tanaka, J. Phys. Chem. B **110**, 8258 (2006).
[28] F. Tielens, M. Calatayud, A. Beltrán, C. Minot, and J. Andrés, J. Electroanal. Chem. **581**, 216 (2005).
[29] H. Iddir, S. Ögüt, P. Zapol, and N. D. Browning, Phys. Rev. B **75**, 073203 (2007).
[30] L. Gracia, J. Garcia-Cañadas, G. Garcia-Belmonte, A. Beltrán, J. Andrés, and J. Bisquert, Electrochem. Solid-State Lett. **8**, J21 (2005).
[31] L. Gracia, M. Calatayud, J. Andrés, C. Minot, and M. Salmeron, Phys. Rev. B **71**, 033407 (2005).
[32] G. W. Peng, A. C. H. Huan, E. S. Tok, and Y. P. Feng, Phys. Rev. B **74**, 195335 (2006).
[33] V. W. J. Verhoeven, I. M. de Schepper, G. Nachtegaal, A. P. M. Kentgens, E. M. Kelder, J. Schoonman, and F. M. Mulder, Phys. Rev. Lett. **86**, 4314 (2001).
[34] Z. Lodziana and J. Piechota, Phys. Rev. B **74**, 184117 (2006).
[35] G. H. Vineyard, J. Phys. Chem. Solids **3**, 121 (1957).
[36] A. Van der Ven, G. Ceder, M. Asta, and P. D. Tepesch, Phys. Rev. B **64**, 184307 (2001).
[37] S. Takai, M. Kamata, S. Fujine, K. Yoneda, K. Kanda, and T. Esaka, Solid State Ionics **123**, 165 (1999).
[38] M. Wilkening, R. Amade, W. Iwaniak, and P. Heitjans, Phys. Chem. Chem. Phys. **9**, 1239 (2007).